OXFORD

Cerebral Cortex, 2025, **35**, bhaf164
https://doi.org/10.1093/cercor/bhaf164
Advance access publication date 15 July 2025
Original Article

Neural and behavioral entrainment to auditory rhythmic perturbations in persons with cerebellar impairment

Eleonora Baliviera[1,†], Mattia Rosso[2,3,†], Bart Moens[3], Marie Poncelet[1], Mario Manto[4], Pierre Cabaraux[5], Bart Van Wijmeersch[1,6], Marc Leman[3], Peter Feys[1,6], and Lousin Moumdjian[1,3,6,*]

[1]REVAL Rehabilitation Research Center, Faculty of Rehabilitation Sciences, Hasselt University, Wetenschapspark 7, 3590 Diepenbeek, Belgium
[2]Center for Music in the Brain, Department of Clinical Medicine, Aarhus University and The Royal Academy of Music, Aarhus/Aalborg, 8000 Aarhus, Denmark
[3]IPEM Institute for Psychoacoustics and Electronic Music, Ghent University, Miriam Makebaplein 1, 9000 Ghent, Belgium
[4]Service des Neurosciences, University of Mons, Avenue du Champ de Mars 8, 7000 Mons, Belgium
[5]Neurological Rehabilitation Ward, Department of Neurology, Hôpital Universitaire de Bruxelles, Université Libre de Bruxelles, Route de Lennik 808, 1070 Brussels, Belgium
[6]University Multiple Sclerosis Centre, Campus Diepenbeek, Agoralaan, 3590, Campus Pelt, Beomerangstraat 2, 3900, Overpelt, Belgium
*Corresponding author: Lousin Moumdjian, Rehabilitation Research Center, Faculty of Rehabilitation Sciences, Hasselt University, Wetenschapspark 7, 3590, Diepenbeek, Belgium. Email: lousin.moumdjian@uhasselt.be
†Eleonora Baliviera and Mattia Rosso shared first authors.

The cerebellum plays a key role in temporal processing, as demonstrated by sensorimotor synchronization paradigms. This study extends findings by investigating behavioral and neural adaptation to unpredictable auditory perturbations. Sixteen persons with cerebellar impairment and sixteen healthy controls performed a listening (60 seconds) and a finger-tapping task (465 seconds) to a metronome set at 1.67 Hz: the first 60 seconds were without perturbations, followed by 40 perturbations (±10% period changes). Event-related frequency adjustments (ERFA) were derived from finger-tapping and electroencephalography recordings, yielding 3 event-related frequency adjustments: one behavioral and two neural (perceptual and sensorimotor components). Mean behavioral adaptation to the perturbations was similar in both groups ($P < 0.001$). Neural tracking was evident in the sensorimotor component but not in the perceptual component in both groups, for both positive ($P = 0.005$) and negative ($P = 0.003$) directions. Neural tracking was significantly reduced in persons with cerebellar impairment compared to healthy controls, particularly in response to negative perturbation in the sensorimotor component ($P = 0.02$). Persons with cerebellar impairment demonstrates spared yet dissociative adaptation with intact behavioral yet hindered neural dynamics. The results suggest parallel yet distinct mechanisms for processing covert and overt responses underlying sensorimotor adaptation. Findings indicate a potential use of spared behavioral adaptation mechanisms in the rehabilitation of persons with cerebellar impairment through rhythm-based interventions.

Keywords: adaptation; cerebellum; EEG; entrainment; event-related frequency adjustments.

Introduction

The cerebellum is a subcortical structure anatomically and functionally well differentiated and is strongly connected with multiple brain regions including thalamic nuclei and cerebral cortex (Voogd 2003). The cerebellum is known for its role in temporal processing (Ivry et al. 2002; Mitoma et al. 2018; Bares et al. 2019; Gatti et al. 2021), facilitating sensorimotor coordination (Molinari et al. 2007). To study the cerebellum's role in the abovementioned functions, perceptual and sensorimotor synchronization paradigms are often used. These paradigms involve perceptual activities like listening to rhythmic patterns, and sensorimotor tasks such as finger-tapping to paced auditory rhythms. These tasks evaluate the following mechanisms: for the listening tasks, these are the perceptual processes involved in extracting temporal regularities from rhythmic structures, forming mental models of these temporal structures and generating temporal predictions (van der Steen and Keller 2013). The sensorimotor synchronization tasks, on the other hand, involve not only these perceptual processes but also additional adaptive mechanisms. These mechanisms engage the motor system to respond to the internalized temporal structures and achieve synchronization (van der Steen and Keller 2013).

Perceptual processing of rhythm in cerebellar pathology has been previously investigated using the frequency tagging approach, which examines the neural response to beat perception using electroencephalography (EEG) recordings during auditory listening tasks (Nozaradan et al. 2011; Nozaradan et al. 2012a; Nozaradan 2014; Nozaradan et al. 2015). This method has been applied to individuals with cerebellar and basal ganglia lesions, and findings indicated that individuals with cerebellar lesions were able to encode the beat at regular tempi but failed to do so at faster tempi (Nozaradan et al. 2017). This is in line with evidence for the cerebellum's role in the precise encoding of temporal events (Ivry et al. 2002; Kotz et al. 2014; Molinari et al. 2007). Furthermore, finger-tapping tasks requiring adaptation to periodic perturbations in rhythmic stimuli have been used to assess sensorimotor synchronization abilities (van der Steen et al. 2015; Schwartze et al. 2016). These studies demonstrated that individuals with cerebellar lesions can correct errors through

Received: January 19, 2025. **Revised:** June 1, 2025. **Accepted:** June 2, 2025

period but not phase adjustments, highlighting deficits in adaptation mechanisms (Schwartze et al. 2016).

On a neural level, in the context of rhythm processing, neural entrainment is defined as the unidirectional synchronization of neural oscillations to an external rhythmic stimulus (Haegens and Zion Golumbic 2018; Lakatos et al. 2019). Its theoretical foundations are grounded in the dynamic attending theory (Large and Snyder 2009; Large et al. 2015), and it has been empirically demonstrated during sensorimotor synchronization tasks (Rosso et al. 2021a; Rosso et al. 2022). Recently, neural entrainment has been quantified in healthy controls (HCs) by the event-related frequency adjustment (ERFA), within a finger-tapping experimental paradigm where participants are presented with rhythms incorporating dynamic frequency changes (Rosso et al. 2023a). ERFA quantifies the frequency adaptations in an oscillatory signal required to respond to these changes at both behavioral and neural levels (Rosso et al. 2023a). This is a novelty, as ERFA allows the comparison of both behavioral and neural responses derived from the same computational framework applied to distinct signals. In addition, ERFA provides the possibility to distinguish the contributions of perceptual and sensorimotor processes to neural responses by means of spatial filters. Specifically, baseline measurements can be conducted to isolate these processes: a listening task to assess perceptual processing and a tapping task in response to auditory stimuli to evaluate sensorimotor processing. These baseline tasks enable the extraction of distinct neural entrainment components, whose dynamics can subsequently be analyzed within the context of the complete sensorimotor task. This approach provides insights into the specific contributions of the perceptual and sensorimotor processes, particularly in adapting to period changes randomly occurring within a rhythmic task. Overall, this methodology helps to address the limitations of the aforementioned studies, which, despite providing valuable insights into cerebellar functioning, still have notable constraints. These include the inability to capture adaptive oscillatory dynamics underlying stimulus processing over time (i.e. neural entrainment) (Rajendran and Schnupp 2019), and the use of gradually changing tempi, resulting in predictable perturbations.

This study aims to investigate behavioral and neural entrainment in persons with cerebellar impairment (PwCI) compared to HCs. Particularly, we focus on examining the behavioral and neural adaptations in response to unpredictable perturbations in rhythm, encompassing both faster and slower perturbations during the synchronization task in this population, and to quantify the adaptive responses as ERFAs. Based on evidence of impaired auditory processing in neurological patients compared to HCs (Vanbilsen et al. 2023) and deficits in encoding at very fast tempi in cerebellar patients (Nozaradan et al. 2017), we hypothesized that cerebellar patients would exhibit reduced behavioral adaptation and neural tracking compared to HCs, particularly for the faster perturbations. We anticipated observing this response at both the behavioral and neural levels. However, we hypothesized that the neural adaptation would be more prominent in the sensorimotor component rather than the perceptual component, as previously observed in HCs (Rosso et al. 2023a).

Materials and methods

Participants

This case–control study was approved by the Medical Ethical Committee of Hasselt University and the local ethical committee of C.H.U. Charleroi and Erasme Hospital Brussels (B1152021000003), the National MS Center Melsbroek and the Rehabilitation and MS center Noorderhart (B1152020000011). The study was registered in the European clinical trial registry (NCT04887753, NCT04639401).

Participants recruited were PwCI and HCs. The following inclusion criteria were used for cerebellar impaired persons: the presence of cerebellar impairment diagnosed by a neurologist evidenced through MRI imaging (presence of a lesion and/or degeneration), or a minimum score of 1 on the Scale of Assessment and Rating of Ataxia (SARA). Participants were excluded when presenting: cognitive impairment impeding understating of instructions, uncorrected hearing impairment, beat amusia, and pregnancy. Eligible patients were asked to sign the informed consent and were invited to participate in two sessions: a descriptive testing session and an experimental session.

The descriptive session

Descriptive tests were collected in a separate session and included general demographic and disease information. The subscales of the rhythm of the Montreal Battery for Amusia were conducted to evaluate amusia (Peretz et al. 2003). Additionally, the following tests were conducted: SARA, to evaluate the presence of ataxia with simple motor commands (stance, sitting, gait and others (Schmitz-Hubsch et al. 2006) and Nine Hole Peg Test (9HPT) to evaluate manual dexterity of both hands, defined as the ability to manipulate small objects using fine hands movement (Oxford Grice et al. 2003). To evaluate cognitive functioning, the CCAS/Schmahmann syndrome scale was administered. This scale is specific to the cerebellar population, developed to evaluate the presence of the cerebellar cognitive affective syndrome (Hoche et al. 2018), by evaluating the following domains: executive function, memory and learning abilities, linguistic abilities and visuo-spatial abilities (Hoche et al. 2018).

The experimental session

Experimental set-up

Participants were sitting in a comfortable chair, facing a table with the custom-made pad containing a strain gage pressure sensor to record finger-tapping onsets. Metronomes were presented auditorily via DefenderShield® air tube earbuds, and the volume was set by the participants before starting the experimental tasks. EEG signal was recorded with an ANT-Neuro eego™ mylab system at a sampling rate of 1 kHz. Each participant wore an EEG headset with 64 electrodes (64-channel waveguard™ original with Ag/AgCl electrodes). A referential montage was chosen, with "Cpz" set as reference for all the electrodes. Impedances were monitored in the eego™ software environment and kept below 20 kΩ. The stimuli sequences were played by a software designed specifically for the experiment, developed in Max MSP 8 (Cycling "74, USA), and run on the stimulation computer (Windows 10, Intel core i7 8th gen, Focusrite Rednet PCIExpress ASIO low-latency soundcard). Perturbations" sequences were randomized for each trial.

Experimental tasks

Participants underwent one listening task without perturbations and one finger-tapping task with perturbations as shown in Fig. 1. The stimuli used throughout the experiments were metronomes set at 100 bpm (1.67 Hz).

The "listening task" lasted 60 seconds and was used to record brain activity as a baseline in the absence of movement, in order to design a spatial filter to extract a perceptual component attuned to the stimulation frequency (Rosso et al. 2023a). To ensure participants paid attention to the stimuli during this listening task, a

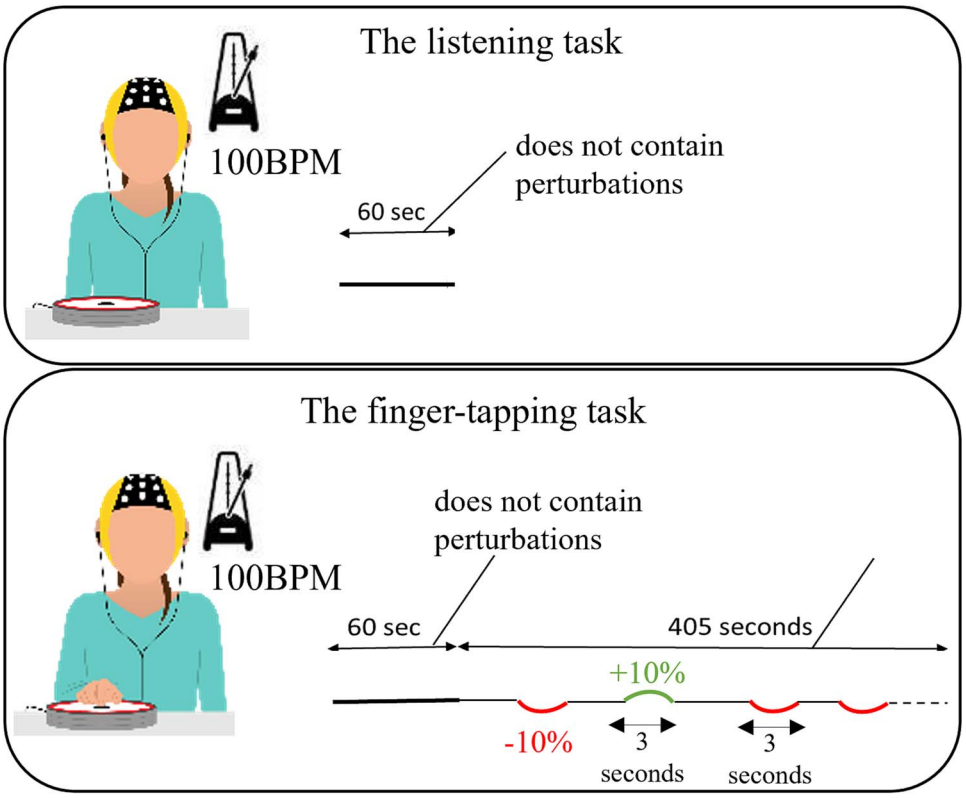

Fig. 1. An overview of the experimental paradigm. A metronome was used as stimuli, and presented at a frequency of 100 beats per minute (1.67 Hz). Participants conducted a listening (60 seconds) and a finger-tapping (465 seconds) task. The finger-tapping tasks included a 60-second perturbation free period, followed by 405 seconds including perturbations lasting 3-secons windows. In total 40 perturbations were presented, divided into 20 perturbations in the negative direction (period change of −10%) and 20 perturbations in the positive direction (period change of +10%). Participants were instructed to synchronize their finger taps with the metronome throughout the entire trial. The period changes shown here are conceptual toy examples, illustrating the expected transient adjustments in response to perturbations. The examples are not meant to be faithful to the actual response trajectories.

clear shift in the rhythm was inserted at the end of the listening task. We instructed participants to sit comfortably, with their hands stretched on the table next to the tapping pad. In order to ensure their active listening, we asked them to stay still and to tap as quickly as possible once when they detected a change in the stimuli, which occurred shortly after 60 seconds. All participants successfully identified and responded to this shift, confirming their engagement in the listening task.

Participants then underwent a "finger-tapping task" with period (i.e. tempo) changes. The finger-tapping task lasted 465 seconds in total, starting with 60 seconds without perturbations to induce a stable behavioral synchronization and a stable sensorimotor oscillation attuned to the stimulus frequency (Rosso et al. 2023a). This was followed by 405 seconds during which perturbations were intermittently introduced. Period changes consisted of +/− 10% step change with respect to the baseline tempo (100 bpm, 1.667 Hz), sustained for 3 seconds before returning to the baseline tempo in a second step. In total, 40 perturbations were presented in a randomized order throughout the task, consisting of 20 negative and 20 positive changes.

Please see the Supplementary audio files containing short excerpt of the metronome stimuli illustrating period perturbations in both positive and negative directions. During the finger-tapping task, participants were informed that there would be changes in the rhythm of the metronomes and were instructed to continuously synchronize in response to the changes in the rhythm they heard. We also instructed them to limit body movements as much as possible to minimize noise in the EEG signal.

Behavioral analysis

Asynchrony and inter-tap-intervals

For each participant, the absolute tap-beat asynchrony and the inter-tap-interval (ITI) were computed separately for trials without perturbations, and trials with perturbations.

Absolute asynchrony was defined as the time difference between each tap and its corresponding beat as the following:

$$\text{Asynchrony}_i = \text{Tap}_i - \text{Beat}_i$$

$$\text{Absolute Asynchrony}_i = |\ \text{Asynchrony}_i\ |$$

And the mean and standard deviation (SD) of the absolute asynchrony was computed as the following:

$$\text{Mean Absolute Asynchrony} = \frac{1}{N}\sum_{i=1}^{N} |\ \text{Asynchrony}_i\ |$$

$$\text{SD Absolute Asynchrony} = \sqrt{\frac{1}{N-1}\sum_{i=1}^{N}\left(|\ \text{Asynchrony}_i\ | - |\ \overline{\text{Asynchrony}}\ |\right)\hat{}2}$$

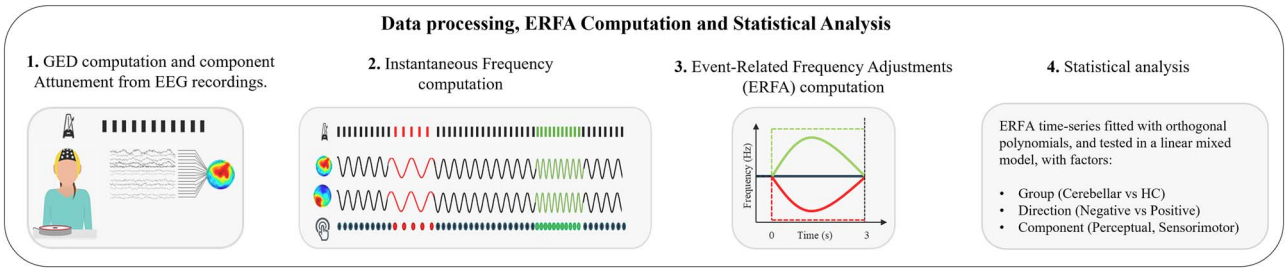

Fig. 2. Data processing, ERFA computation and statistical analysis workflow. This workflow replicated methodology from previous work[22]. *Step 1*. An attunement phase was conducted under active listening and finger-tapping during a perturbation-free auditory metronome for 60 seconds. Using these two datasets, two spatial filters were designed per participant to extract a purely perceptual (without movement) and a sensorimotor (with movement) entrained oscillatory components, respectively. *Step 2*. Participants underwent 405 containing alternating time-windows of perturbation-free and perturbated events. Examples of negative (red) and positive (green) perturbation windows are represented illustrating how the metronomes' onset were manipulated and how neural components and finger-taps were expected to entrain. The entrained oscillatory components were narrow-band filtered around the metronome's center frequency and Hilbert-transformed to produce analytic signals and extract phase timeseries. These were then unwrapped to prevent phase resets, differenced and scaled to Hz to produce instantaneous frequency timeseries, namely an estimate of the oscillation's frequency at every timepoint. *Step 3*. Instantaneous frequency timeseries were segmented based on perturbation windows, and aggregated by perturbation direction. The average of the event-based segments provided the outcome measure ERFA: one for the behavior and two for the neural components (perceptual and sensorimotor). The continuous lines in *Step 3* illustrate the response expected when ERFA curve tracks the stimulus dynamic and direction. The dashed lines represent the stimulus dynamic during negative (red) and positive (green) perturbations. *Step 4*. Orthogonal polynomials with a linear and a quadratic term were used to model the ERFAs. Data were then fitted in a linear mixed model, with random effect of participants and fixed effects of group, direction and, only for the neural ERFA, components.

ITI was calculated as the time difference between successive taps, and thereafter the mean and SD was computed as the following:

$$\mathrm{ITI}_i = \mathrm{Tap}_{i+1} - \mathrm{Tap}_i$$

$$\text{Mean ITI} = \frac{1}{N-1}\sum_{i=1}^{N-1}\mathrm{ITI}_i$$

$$\text{SD ITI} = \sqrt{\frac{1}{N-2}\sum_{i=1}^{N-1}\left(|\,\mathrm{ITI}_i\,| - |\,\overline{\mathrm{ITI}}\,|\right)\text{^}2}$$

Interpolation

Finger-tapping data were subsequently interpolated with the aim of obtaining instantaneous frequency time series to align with the neural ERFAs, expressed in the same unit of measure (Hz). The intervals between the remaining timestamps were linearly interpolated from 0 to 1 at a 1 kHz sampling rate. The resulting ramp wave was scaled to 2π, providing an estimate of the finger-taps phase with a temporal resolution of 1 ms. Instantaneous frequency time series were computed as the first derivative of the unwrapped phase angles time series (Boashash 1992), and converted to Hz with the following formula (Cohen 2014):

$$Hz_t = \frac{s\,(\phi_t - \phi_{t-1})}{2\pi}$$

Unwrapping was necessary for removing discontinuities in the time series caused by phase resets.

EEG analysis

Figure 2 provides a summary of the workflow involving the signal processing steps leading to the computation of ERFA curves. This workflow is a direct replication of one previously developed and validated in recent work (Rosso et al. 2023a).

Data-processing

EEG data were pre-processed using a set of functions from the *Fieldtrip* toolbox (Oostenveld et al. 2011) for Matlab for the visual inspection of bad channels, whose removal was conducted manually for each participant. A six-order Butterworth high-pass filter with a 1 Hz cut-off was applied to remove slow drifts; a low-pass sixth-order Butterworth filter with a 40 Hz cut-off to remove high-frequency muscular activity; a fourth-order notch filtered at 50 Hz to remove power-line noise up to the third harmonic. Notch filtering was included despite the low-pass cut-off at 40 Hz to fully replicate the previous analysis pipeline to suppress any residual power line noise, as it is common practice and does not negatively impact signal quality (Rosso et al. 2023a). Subsequently, independent component analysis (ICA) as implemented in the "runica" "Fieldtrip" algorithm was conducted to remove artifactual components by means of visual inspection of both topographical maps and activation time series. The reference "CPz" and the bad channels' time series were excluded from the input matrix. Components which exhibited the stereotypical frontal distribution generated by blinks and lateral eye movements, or bilateral temporo-mastoidal distribution with periodic peaks in the activation time series plausibly generated by heart beats were removed. Extra components were removed in instances where recurrent artifacts with clearly abnormal amplitude were detected. The dataset was inspected prior to ICA decomposition and following ICA back-projection to assess the quality of the artifact removal. Rejected bad channels were reconstructed after artifact removal, by computing the average activity from neighboring electrodes indicated by the template provided by ANT Neuro for 64-channel waveguard™ original caps.

Generalized Eigendecomposition

Source separation was conducted via generalized Eigendecomposition (GED) (Cohen 2022) to extract the perceptual and the sensorimotor components attuned to the rhythmic stimulus frequency. GED allows to optimize the signal-to-noise ratio between the entrained component and the broadband neural activity, working as a spatial filter to separate sources and reduce data dimensionality. The spatial filter consisted of a set of vectors W (weights) calculated by solving the following:

$$RW\Lambda = SW$$

where S is the covariance matrix of the narrow-band signal; R is the reference covariance matrix of the broad-band signal; Λ is

the set of eigenvalues. The eigenvector associated with the largest eigenvalue was taken as a spatial filter, transposed and multiplied by the broadband data matrix to reconstruct the time series of our target entrained components.

GED identifies eigenvectors W that best separate the signal (S) covariance from the reference (R) covariance matrix. The S covariance matrix was computed from the narrowband signal, the R covariance matrix was here computed from the broadband multivariate signal. In order to narrow-band filter the data, we designed our filter as a Gaussian function in the frequency domain, with center at 1.667 Hz and a width of 0.3 Hz at half of the maximum. We then filtered the broadband data at all channels via element-wise multiplication between broadband signal and wavelet kernel in the frequency domain, and transformed the resulting narrowband signal back in the time domain with inverse fast Fourier transform. Covariance matrices were computed within 600 ms time windows locked to the finger-taps onsets, and grand average S and R covariance matrices were computed. The individual matrices whose z-normalized Euclidean distance from the grand average exceeded the 2.23 z-scores, and the grand average S and R recalculated. 1% regularization was applied to R.

GED was applied separately for each individual participant to optimize the spatial filter accounting for individual variability in the scalp projections of the underlying oscillatory components. The spatial filter for the Perceptual component was computed from 60 seconds of listening task, while the spatial filter for the Sensorimotor component was computed from the first 60 seconds of the finger-tapping task (non-perturbated). The actual components time series (y) were computed by multiplying the eigenvector (w) associated with the highest eigenvalue by the broadband EEG data (X) recorded during the 405 seconds of perturbation task:

$$y = w^T X$$

The associated spatial activation pattern, namely the spatial projection of the component over the scalp, was computed as follows:

$$a = w^T S$$

Finally, to extract reliable phase timeseries from the GED components, these were narrow-band filtered using the same Gaussian filter (center at 1.667 Hz; full width at half-maximum of 0.3 Hz). The analytic signal was computed via Hilbert transform, which enabled to compute its phase. Provided phase timeseries, instantaneous frequency was calculated:

$$Hz_t = \frac{s\,(\phi_t - \phi_{t-1})}{2\pi}$$

Supplementary Fig. 1 shows the quality of the GED source separation application in both groups.

ERFA

Provided the instantaneous frequency timeseries computed over the continuous recording, ERFA curves were computed for both neural components (extracted via GED from the EEG signal) and behavioral time series (from finger-tapping) in order to express changes in instantaneous frequency in response to stimulus perturbations (Rosso et al. 2023a). ERFAs were expressed as the percentage of frequency change per unit time, relative to the baseline frequency preceding the perturbation. Behavioral, perceptual (neural) and sensorimotor (neural) ERFAs were computed for each perturbation, in each condition, for each participant.

ERFA curves were derived by averaging these dynamic frequency changes across events, separately for positive (+10% change) and negative (−10% change) perturbations. In order to compute the statistical significance of the frequency changes, a baseline ERFA was computed as the average frequency change in the stable periods preceding the perturbations (0% change). Perturbation onsets were identified based on the timestamp logs of the events. ERFA time windows were defined from −500 to +3,000 ms with respect to the perturbation onset, aggregated per perturbation type and direction, baseline-normalized and averaged. Baseline normalization was performed by subtracting the average of the 500 to 0 ms interval from the rest of the ERFA, dividing by the target stimulation frequency (i.e. 1.667 Hz) and multiplied by 100. The resulting ERFA is expressed in percent change with respect to the baseline stimulation frequency.

Since the neural oscillatory components were attuned to the stimulation frequency (1.667 Hz) and filtered with a 0.3 Hz bandwidth, the filter enabled the extraction of reliable instantaneous phase timeseries while allowing for frequency deviations within the filter's passband. Systematic deviations from the baseline stimulation frequency were expected as the result of the ±10% tempo perturbations introduced during the task. While the stimulation frequency was fixed at 1.667 Hz, the entrained neural oscillations were hypothesized to adjust dynamically in response to the perturbations before returning to the baseline. This approach enabled us to capture event-locked adjustments in neural and behavioral frequency during the perturbation windows.

In order to ensure the same number of events across participants, the final perturbation was excluded for all participants due to occasional missing log data. Thus, ERFA curves were averaged across the initial 19 perturbations, aggregated per type (negative and positive). Negative perturbation responses were sign-flipped to enable direct magnitude comparison with positive perturbations in our statistical model (Jantzen et al. 2018; Rosso et al. 2023a). Further methodological details of the ERFA paradigm are described in previous work involving healthy participants (Rosso et al. 2023a).

Statistical analysis

To analyze descriptive tests, a two-sample Wilcoxon test was applied to the responses across groups as data were not normally distributed. To analyze the effects of experimental conditions on mean and SD of asynchrony and ITI, a linear mixed effects model was fitted per outcome, with participant as a random effect, and main effects of Group (PwCI and HC) and Trials (no perturbation and perturbation). Specific to the ERFAs, the response variables were the behavioral, the neural perceptual, and the neural sensorimotor ERFAs. We also analyzed the SD of the behavioral ERFAs in order to quantify the variance of responses across groups and perturbation directions. ERFA curves were expected to track the stimulus dynamics, expressed in terms of instantaneous frequency. Therefore, as shown in Fig. 2 step 3, the ERFA curves were expected to have a gradual and sustained response to period changes as a response to tracking the stimulus dynamic and direction. For the analysis of the experimental conditions, growth curve analysis (Mirman 2017) was used to model the changes in instantaneous frequency of the neural entrained component. Orthogonal polynomials model the changes in the instantaneous frequency of the entrained components (ERFA) within 3-second perturbed windows (Mirman 2017; Rosso et al. 2021b; Rosso et al. 2023b). We defined our model as a second-order polynomial function, consisting of the following terms: an intercept corresponding to the average of the curve, a linear term corresponding to the slope

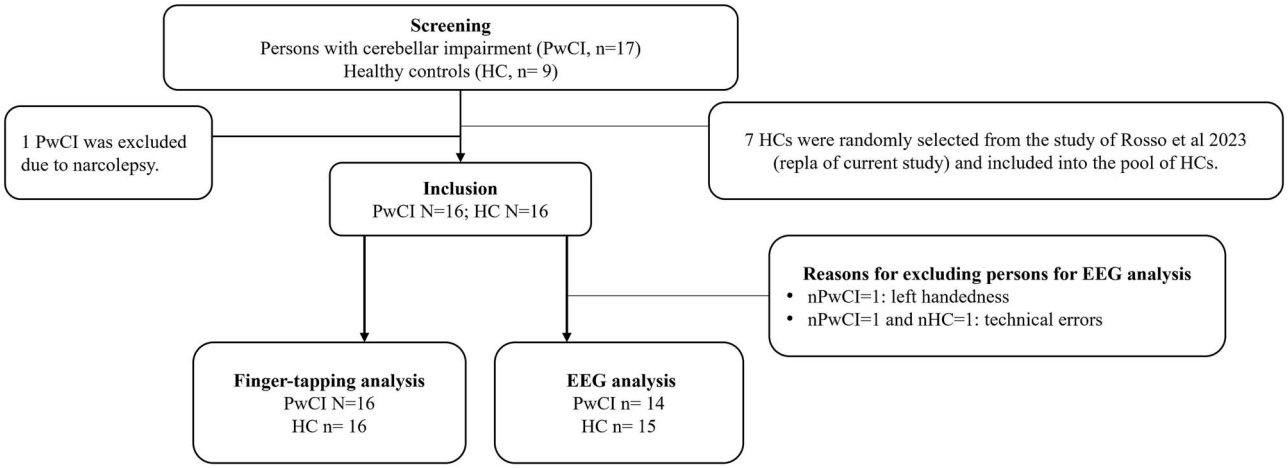

Fig. 3. Experimental flow-chart reporting inclusion and exclusion criteria and the data collection and analysis.

of the curve (Ot1, first order), and a quadratic term corresponding to the depth of its parabolic curvature (Ot2, second order) (Rosso et al. 2023a).

A linear mixed model was fit to each type of ERFA using RStudio, with random effect of participants and fixed effects of Group (PwCI and HC), Direction (Positive and Negative) and Component (Sensorimotor and Perceptual). The latter factor operationalized the distinction between the two neural ERFAs. The model estimates were based on the following reference levels: Null (absence of perturbation) for Direction, HCs for Group, and Perceptual for Component. Post-hoc analysis with Bonferroni correction was conducted when interaction effects were significant, in order to interpret the directionality of the result relative to the baseline. The significance level of 0.05 was used as statistical threshold. The following formulas were used for the models fitted to behavioral and neural ERFAs, respectively (in R syntax):

$$\begin{aligned} Behavioral\ ERFA \sim & \left(Time + Time^2\right) * Direction * Group \\ & + \left(Time + Time^2 \mid Subject\right) \\ & + \left(Time + Time^2 \mid Subject : Direction : Group\right) \end{aligned}$$

$$\begin{aligned} Neural\ ERFA \sim & \left(Time + Time^2\right) * Component * Direction * Group \\ & + \left(Time + Time^2 \mid Subject\right) \\ & + \left(Time + Time^2 \mid Subject : Component : Direction : Group\right) \end{aligned}$$

The study sample was estimated based on our previous work applying the same experimental paradigm to HCs (Rosso et al. 2023a). An a priori power analysis was conducted on the neural sensorimotor ERFA on the positive period perturbation. To achieve a power of 0.75 with an alpha of 0.05 and a beta of 0.25, the analysis determined that 15 participants per group were needed to ensure adequate statistical power.

Results

Participants

The study (see flow chart in Fig. 3) included 16 PwCI, encompassing a range of diagnosis including cerebellar stroke, spinocerebellar ataxia type six, anterior-venous stenosis malformation, cerebellar lesion due to an ischemic, inflammatory or neuropathic cause and multiple sclerosis. All participants except one exhibited mild ataxia, as reflected by their SARA scores (median: 3.0, interquartile range: 2.0–7.0). One participant scored zero on the SARA, indicating the absence of ataxia. The individual medical diagnosis and ataxia rating, as assessed by the SARA, are presented for each participant in Table 1.

Nine HCs were recruited and included in the study, and data from seven HCs were randomly selected from our previous study which applied the same experimental procedure and analysis as the current study (Rosso et al. 2023a). Behavioral data was analyzed in all participants, while EEG data were analyzed in 14 PwCI and 15 HCs, due to technical errors during the recording (nPwCI = 1, nHC = 1) and left-handed dominance (nPwCI = 1).

As seen in Table 2, groups significantly differed in age, but not on gender or on the rhythm subscale test for assessing Amusia. The two groups significantly differed at baseline in terms of the presence of ataxia (SARA total score $z = -3.70$, $P = 0.0002$), and on the 9HPT of the right and dominant hand ($z = -2.61$, $P = 0.008$). The results of the CCAS/Schmahmann syndrome scale test indicated that 8 patients failed on 3 or more tests.

Asynchrony and ITIs

Figure 4A shows the mean and SD for asynchrony (Fig. 4A) and ITIs (Fig. 4B) across perturbation and perturbation-free trials for both groups. There were no significant main effects or interactions for the mean asynchrony or the mean ITI**.** In contrast, a significant main effect of Group was found for the SD of asynchrony ($F[1, 22.1] = 9.20$, $P < 0.0006$), with the patient group exhibiting greater variability than HCs. In addition, in both groups, asynchrony variability was significantly higher during perturbation trials compared to non-perturbation trials ($F[1, 18.5] = 59.39$, $P < 0.0001$). A similar pattern was observed for the SD of ITI, indicating a higher tapping variability in patients than controls ($F[1, 7.8] = 14.56$, $P < 0.005$). In addition, in both groups, higher tapping variability during the perturbation trials compared to the perturbation free trials ($F[1, 9.0] = 66.55$, $P < 0.0001$) was found.

ERFA

Below, the results of the ERFA curves for the behavioral (finger-tapping) and neural (EEG) data are presented. Figure 5 illustrate results visually for PwCI and HCs. Table 3A and 3B provides an

Table 1. Details of diagnosis, MRI findings, age and subscales of the scale for assessment and rating of ataxia.

Diagnosis	Age	Year of diagnosis	MRI finding	Subscales of scale for assessment and rating of ataxia									
				Gait	Stance	Sitting	Speech disturbance	Finger chase		Nose-finger test		Fast alternating hand movements	
								Left	Right	Left	Right	Left	Right
Cerebellar stroke	62	2018	Left posterior cerebellar stroke (superior cerebellar artery)	1	0	0	0	1	0	0	0	1	0
Spinocerebellar ataxia type 6	65	2017	Global cerebellar atrophy predominantly cerebellar vermis	3	2	0	2	0	0	1	1	1	1
Cerebellar stroke	73	2019	Right posterior paravermis stroke (posterior inferior cerebellar artery)	1	1	0	0	0	0	0	0	0	0
Cerebellar Stroke	62	2021	Right posterior paravermis stroke (posterior inferior cerebellar artery)	1	0	0	0	0	0	0	0	0	0
Cerebellar stroke	54	2021	Multiple lesions of bilateral cerebellar hemispheres	1	0	0	0	0	0	1	0	0	0
Anterior-venous stenosis malformation	28	2009	Bilateral posterior cerebellar hemispheric lesions and mild cerebellar atrophy	1	0	0	0	0	0	0	0	0	0
Cerebellar stroke	46	2019	Left hemispheric cerebellar stroke	2	1	0	1	1	0	1	0	1	0
Cerebellar stroke	78	2019	Bilateral posterior inferior cerebellar artery stroke	1	2	0	0	0	0	0	0	0	0
Ischemic, inflammatory or neuropathic cause	69	2020	Left middle cerebellar peduncle lesion	0	0	0	0	0	0	0	0	0	0
Cerebellar stroke	77	2019	Ischemia in left posterior cerebellar hemisphere (anterior superior cerebellar artery)	1	0	0	0	1	1	0	0	0	0
Relapsing Remitting multiple sclerosis	42	2022	Lesion at the left cerebellar peduncle and in the right cerebellar hemisphere body	0	0	0	0	0	0	1	1	0	0
Relapsing Remitting multiple sclerosis	48	2015	Lesion at the left border of 4th ventricle and cerebellar peduncle	1	2	0	0	1	1	0	0	1	1
Multiple Sclerosis	56	2004	No lesions or atrophy observed on imaging	4	1	0	0	0	0	1	1	1	1
Spinocerebellar ataxia type 6	69	2019	Global cerebellar atrophy	7	6	1	3	2	2	2	2	2	2
Cerebellar Stroke	54	2023	Right hemisphere middle and anterior vermis stroke (Right antero-superior cerebellar artery)	1	1	0	0	1	0	1	0	0	0
Cerebellar Stroke	61	2018	Left posterior parasagittal hemisphere stroke (Left postero-inferior cerebellar artery)	1	1	0	0	1	1	1	1	0	0

Table 2. Descriptive results with mean and SD for demographic, motor, cognitive and amusia tests divided by group (cerebellar patients and HCs).

	Cerebellar patients ($n = 16$) Mean ± SD	HCs ($N = 16$) Mean ± SD	*t*-test or Wilcoxon test or χ^2 (*P*-value)
Age (year)	59.25 ± 12.92	48.19 ± 17.05	$t = -2.06$, $P = 0.05$
Gender (female; male)	8; 8	10; 6	$\chi^2 = 0.508$, $P = 0.48$
Montreal battery for evaluation of amusia, rhythm subscale[c]	12.92 ± 1.80	13.14 ± 1.46	$Z = 0.04$, $P = 0.97$
Scale for assessment and rating of ataxia; total score[c]	4.63 ± 6.11	0.00 ± 0.00	$Z = -3.70$, $P = 0.0002$[b]
Nine hole peg test; right hand (seconds)[c]	26.48 ± 7.42	20.52 ± 2.14	$Z = -2.61$, $P = 0.008$[b]
Nine hole peg test; left hand (seconds)[c]	30.76 ± 14.29	22.78 ± 2.43	$Z = -1.90$, $P = 0.06$
Cerebellar cognitive affective scale; total score	78.93 ± 30.78	–	–

[a] $P < 0.05$. [b] $P < 0.01$. [c] These tests include $n = 9$ HC.

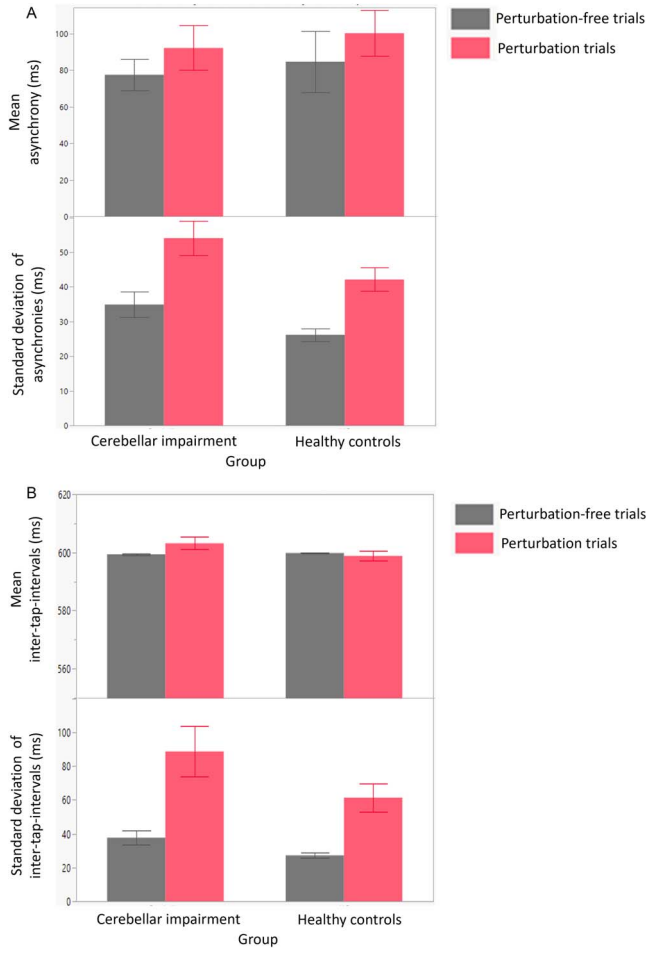

Fig. 4. (A) Group-level means and SDs for asynchrony across perturbation-free and perturbation trails. Error bars indicate the standard errors of the mean (SEM). (B) Group-level means and SDs for ITIs across perturbation-free and perturbation trails. Error bars indicate the standard errors of the mean (SEM).

overview of the statistical results observed on the behavioral and neural ERFA measures respectively.

Behavioral ERFA (mean)

A significant main interaction effect was found between the quadratic component (Ot2) and the two directions: positive (estimate = −86.05, SE = 9.55, $P < 0.001$) and negative (estimate = −86.96, SE = 9.39, $P < 0.0001$), indicating that both groups adapted their finger-taps in accordance to the perturbation direction (i.e. faster for the positive tempi, and slower for the negative direction).

Behavioral ERFA (SD)

A significant main effects of Direction was found for the Negative perturbation (estimate = −18.81, $P < 0.0001$), indicating a lower variability in the ERFA time course during the Negative perturbations. A significant interaction between the linear component (Ot1) and Negative perturbation Direction (estimate = −25.61, $P = 0.02$) indicated that the slope of the ERFA response—reflecting the initial rate and direction of adaptation—was with less variability in linear responses during the Negative direction. A three-way interaction was found between the linear component (Ot1), perturbation direction, and group (estimate = 33.10, $P = 0.03$) showing that PwCI exhibited greater variability in their linear response during Positive perturbation direction compared to HCs.

Neural ERFA

A significant two-way interaction effect was found between the quadratic component (Ot2) and Direction for Positive and Negative (positive: estimate = −10.96, SE = 4.17, $P = 0.009$; negative: estimate = −12.49, SE = 4.17, $P = 0.003$), indicating that both groups entrained at a neural level with the stimuli according to the perturbation's direction.

A significant two-way interaction effect was found between Group and Direction, indicating that PwCI responded with a less prominent parabolic curve than HC for the Negative direction (Estimate = −1.96, SE = 0.60, $P = 0.001$).

A significant three-way interaction effect was found between the quadratic component Ot2 and the sensorimotor component, in both perturbation directions (positive: estimate = −16.55, SE = 5.90, $P = 0.005$; negative: estimate = −17.62, SE = 5.90, $P = 0.002$). This indicates that, compared to the Perceptual component, the Sensorimotor component increased the parabolic curvature when perturbations occurred, regardless of the Direction.

A significant three-way interaction effect was found between the quadratic component Ot2, the cerebellar group and in both perturbation directions (positive: estimate = 14.38, SE = 5.99, $P = 0.016$; negative: estimate = 14.39, SE = 5.99, $P = 0.016$). This indicates the presence of lower frequency adjustment in PwCI compared to HCs, regardless of direction. post-hoc tests revealed a significant interaction between group and component (estimate = 1.291, SE = 0.299, z ratio = 4.325, $P < 0.0001$), indicating that PwCI (meanEstimate= 0.459, SE = 0.214) has less prominent frequency adjustment in the sensorimotor component compared to HCs (meanEstimate = 1.750, SE = 0.208).

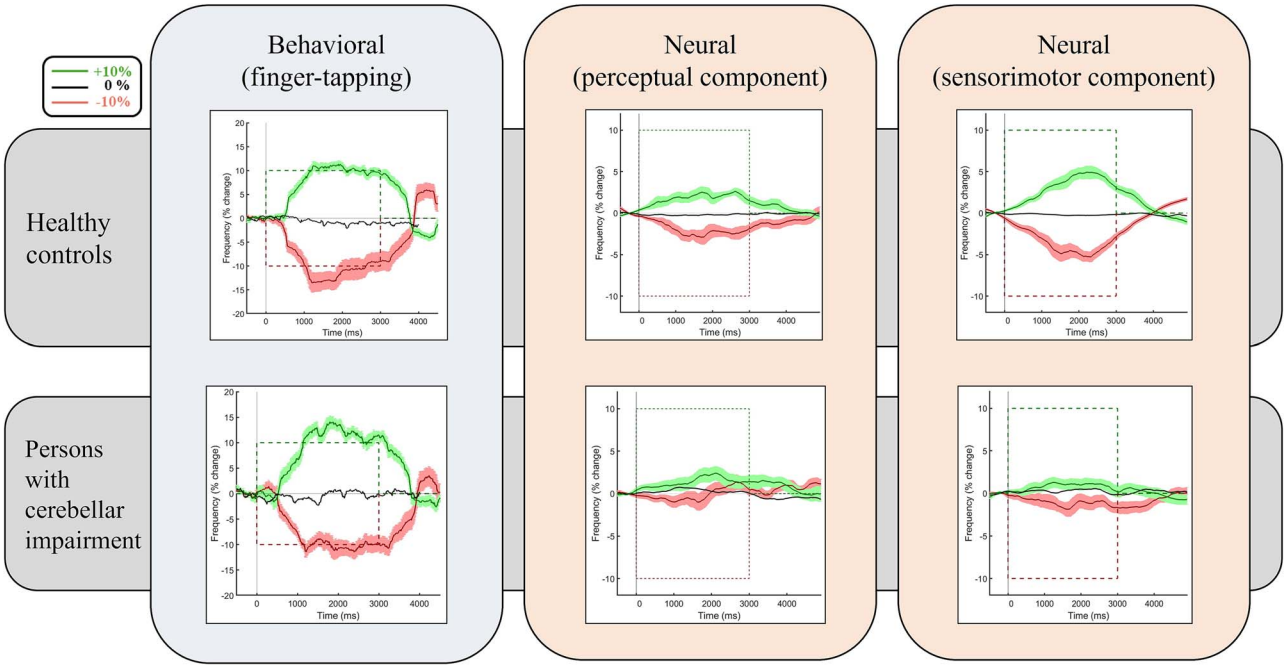

Fig. 5. Grand averages of ERFA curves. Grand averages of the ERFA curves for period changes for both the groups. The x-axis represents time, and the y-axis represents the percentage of frequency change from the pre-stimulus baseline following the perturbation onset. The figures on the top panel represent grand averages for HCs, distinguished by behavioral and neural ERFA (with the two components, perceptual and sensorimotor). The figures on the bottom panel represent grand averages for PwCI, distinguished by behavioral and neural ERFA (with the two components, perceptual and sensorimotor). Positive perturbations correspond to the green lines, while negative perturbations correspond to the red lines. The auditory stimuli presented is represented by the dashed lines, while the results observed is represented by the solid lines, with shadings illustrating the standard error of the means. Neural ERFA responses appear smoother and return to baseline earlier compared to their behavioral counterparts due to temporal smoothing introduced by narrow-band filtering of EEG data, an inherent artifact of the filtering necessary for accurate instantaneous frequency estimation. Importantly, this smoothing does not affect the validity of the results, as statistical comparisons are carried out separately for the neural and behavioral domains.

A significant four-way interaction was found between the linear component Ot1 and the sensorimotor component in the positive direction for the cerebellar group (estimate = −16.94, SE = 7.94, $P = 0.03$). This indicates, that compared to HCs, PwCI exhibit a more prominent linear adaptation to perturbations in the positive direction than the negative direction.

Discussion

The present study aimed to investigate the behavioral and neural entrainment of PwCI in response to period perturbations in auditory rhythms, compared to HCs. To achieve this, an experimental paradigm designed was applied to quantify the behavioral and neural dynamics underlying rhythmic tracking, using the ERFA as an outcome measure (Rosso et al. 2023a). This study investigated the ability to adapt to unpredictable perturbations, which differentiates it from previous works focusing on cerebellar patients' ability to synchronize to more predictable incremental period changes (Repp 2005; Nozaradan et al. 2012b; Nozaradan 2014; Nozaradan et al. 2017). The unpredictable nature of our perturbations makes ERFA a particularly informative measure, since it consists of the frequency adjustment of an oscillatory signal in response to a period change (i.e. adaptation).

The study included PwCI of various aetiologies, most of whom exhibited mild ataxia as assessed by the SARA, except for one participant who showed no ataxia. The patient group differed significantly from controls in the variability of asynchrony and inter-tap intervals, reflecting deficits in timing and incoordination associated with cerebellar dysfunction (Manto 2009; Marsden and Harris 2011; Cabaraux et al. 2023). The responses of higher variability in the cerebellar group align with previous study results on sensorimotor synchronization in cerebellar patients (van der Steen et al. 2015; Schwartze et al. 2016), further supporting the presence of subtle timing and coordination deficits, albeit the mild or no clinical presentation of ataxia as assessed by the SARA.

Contrary to our hypothesis, we did not find any significant differences between groups for the mean behavioral ERFAs. This informs us that behaviorally, patients adapted their finger taps to both perturbation directions, achieving a performance comparable to that of the HCs. Thus, they had spared ability to detect and consequently adapt their finger-tapping to unpredictable changes in auditory rhythms. One explanation for this result can be rooted in auditory recognition, which has been shown to be spared in patients with cerebellar patients (McLachlan and Wilson 2017). Particularly, the authors argued that the cerebellum is involved in the implicit learning of spectro-temporal information, used for sound and speech recognition. The stimuli used in this experiment, being the metronomes, are very simple sounds, and thus previously stored sound information could have been used by the patients to automatically recognize incoming sounds and predict subsequent events (McLachlan and Wilson 2017). Another explanation of the spared behavioral response can be placed and explained by the concept of rhythmicity, as a previous study demonstrated that patients with cerebellar degeneration showed sparing of a temporal prediction from cues that were embedded in a rhythmic structure, compared to cues that were presented as a single interval (Breska and Ivry 2018). These assumptions can be tested further by future studies investigating these paradigms in PwCI, using stimuli that vary in both auditory recognition difficulty and rhythmic complexity. Examples of such stimuli can be found in music, which allows for variation in complexity.

Table 3A. Model summary of the behavioral ERFAs: differences across groups (e.g. cerebellar patients vs. HCs), direction (negative vs. positive), and component type (sensorimotor vs perceptual). Categorical predictors are dummy-coded, with estimates shown for each level relative to the baseline (e.g. cerebellar relative to healthy). Negative direction indicates a slowing down of the rhythm, and positive direction indicates a speeding up. Ot1 refers to the linear component of the polynomial fit, while Ot2 reflects the quadratic curvature term of the polynomial fit. Columns report the estimated effect (Est.), standard error (SE), *t*-value (*t*), and *P*-value (*P*).

Outcome measure	Predictors	Estimate	SE	t-value	P-value
Behavioral ERFA (mean)	Positive (+)	7.86	1.14	6.92	<0.001[b]
	Negative (−)	8.73	1.12	7.82	<0.001[b]
	Ot1	−8.85	9.35	−0.95	0.34
	Ot2	5.01	6.82	0.74	0.46
	Cerebellar	0.13	1.23	0.11	0.91
	Ot1:Positive (+)	22.87	12.00	1.91	0.056
	Ot1:Negative (−)	14.25	11.78	1.21	0.22
	Ot2:Positive (+)	−86.05	9.55	−9.01	<0.001[b]
	Ot2:Negative (−)	−86.96	9.39	−9.26	<0.001[b]
	Ot1:Cerebellar	13.46	13.21	1.01	0.31
	Ot2:Cerebellar	−5.46	9.64	−0.57	0.57
	Cerebellar:Positive (+)	0.42	1.58	0.26	0.79
	Cerebellar:Negative (−)	−1.06	1.58	−0.67	0.5
	Ot1:Cerebellar:Positive (+)	−2.45	16.74	−0.15	0.88
	Ot1:Cerebellar:Negative (−)	13.57	16.65	0.81	0.41
	Ot2:Cerebellar:Positive (+)	−3.08	13.30	−0.23	0.82
	Ot2:Cerebellar:Negative (−)	21.30	13.28	1.60	0.11
Behavioral ERFA (SD)	Ot1	14.47	7.68	1.89	0.06
	Ot2	−8.55	5.91	−1.45	0.15
	Positive (+)	0.95	2.85	0.33	0.74
	Negative (−)	−18.81	2.85	−6.59	<0.0001[b]
	Cerebellar	3.71	2.81	1.32	0.19
	Ot1:Positive (+)	−14.44	10.77	−1.34	0.18
	Ot1:Negative (−)	−25.61	10.77	−2.38	0.02[a]
	Ot2:Positive (+)	−11.45	8.35	−1.37	0.17
	Ot2:Negative (−)	6.47	8.35	0.77	0.44
	Ot1:Cerebellar	−7.94	10.71	−0.74	0.46
	Ot2:Cerebellar	−5.35	8.23	−0.65	0.53
	Positive (+):Cerebellar	0.77	3.98	0.19	0.85
	Negative (−):Cerebellar	−7.42	3.98	−1.87	0.06
	Ot1:Positive (+):Cerebellar	33.10	15.01	2.21	0.03[a]
	Ot1:Negative (−):Cerebellar	8.35	15.01	0.56	0.58
	Ot2:Positive (+):Cerebellar	7.26	11.64	0.62	0.53
	Ot2:Negative (−):Cerebellar	16.85	11.64	1.45	0.15

[a] $P < 0.05$. [b] $P < 0.01$.

A higher variability of the behavioral ERFA responses was observed in the positive compared to the negative perturbation direction in all participants during the initial adaptation phase, and this was more pronounced in the patient group. High variability in motor control can reflect active exploration by sensorimotor circuits, enabling the motor system to discover and refine performance through adaptation (Dhawale et al. 2017). Adapting to the positive perturbation direction likely required greater variability because faster rhythmic contexts compress the temporal window for motor planning and execution. The more pronounced variability observed in PwCI compared to HCs during the initial phase of adaptation to positive perturbations may be attributed to coordination impairments characteristic of cerebellar dysfunction (Manto 2009; Marsden and Harris 2011).

Consistent with our hypothesis and previous study (Rosso et al. 2023a), the neural tracking for period changes was found to be more prominent in the sensorimotor component as compared to the perceptual one, in both groups. The additive contribution of the sensorimotor component could potentially be explained by bottom-up resources (i.e. due to the presence of the proprioceptive feedback from the finger taps). Previously, it has been demonstrated that somatosensory feedback, during paced finger-tapping movements, is supported by the activation of the sensorimotor cortex (Pollok et al. 2002). Specific to the sensorimotor component, the results indicate that HCs showed better tracking within the sensorimotor component compared to the cerebellar patient group (see Fig. 5). An explanation for this may be linked to the adaptation and temporal tracking activity governed by a top-down control using feedforward control, which is typically impaired in cerebellar patients (Bastian 2006).

Results of the period changes also show an interaction effect of the perturbation's direction, resulting in worse neural tracking for the negative direction in cerebellar patients compared to HCs. This may be indicative of different functioning of inhibition processes between the groups. In order to track slower rhythms, a person's comfortable motor response needs to be inhibited, as shown in studies applying the stop paradigms (Band and van Boxtel 1999). In our study sample, eight patients failed three or more tests on the CCAS/Schmahmann syndrome scale (Schmahmann 2019), which may be supportive of our interpretation. A further continuation of this line of thought can be linked to the cerebellum's role in forward models, and the hindering of motor performance when feedback is altered (Popa and Ebner 2018). It has been demonstrated that the cerebellum is involved in motor learning, particularly in creating hierarchical generative models used to predict actions (Manto et al. 2012; Popa and Ebner

Table 3B. Model summary of the neural ERFAs: differences across groups (cerebellar patients vs. HCs), direction (negative vs. positive), and component type (sensorimotor vs perceptual). Categorical predictors are dummy-coded, with estimates shown for each level relative to the baseline (e.g. cerebellar relative to healthy). Negative direction indicates a slowing down of the rhythm, and positive direction indicates a speeding up. Ot1 refers to the linear component of the polynomial fit, while Ot2 reflects the quadratic curvature term of the polynomial fit. Columns report the estimated effect (Est.), standard error (SE), *t*-value (*t*), and *P*-value (*P*).

Outcome measure	Predictors	Estimate	SE	t-value	P-value
Neural ERFA	Ot1	1.24	2.76	0.45	0.65
	Ot2	0.51	3.14	0.16	0.87
	Sensorimotor	0.01	0.42	0.03	0.96
	Positive (+)	1.67	0.42	4.00	<0.0001[b]
	Negative (−)	1.85	0.42	4.43	<0.0001[b]
	Cerebellar	0.43	0.46	0.94	0.35
	Ot1:Sensorimotor	−1.24	3.90	−0.32	0.75
	Ot2:Sensorimotor	0.70	4.17	0.17	0.87
	Ot1:Positive (+)	−1.41	3.90	−0.36	0.72
	Ot1:Negative (−)	0.59	3.90	0.15	0.88
	Ot2:Positive (+)	−10.96	4.17	−2.63	0.009[b]
	Ot2:Negative (−)	−12.49	4.17	−2.99	0.002[b]
	Positive (+):Sensorimotor	1.09	0.59	1.85	0.07
	Negative (−):Sensorimotor	1.08	0.59	1.82	0.06
	Ot1:Cerebellar	−6.10	3.97	−1.54	0.12
	Ot2:Cerebellar	−5.36	4.51−	−1.19	0.23
	Cerebellar:Sensorimotor	−0.21	0.60	−0.36	0.72
	Cerebellar: Positive (+)	−0.83	0.60	1.38	0.17
	Cerebellar:Negative (−)	−1.96	0.60	−3.25	0.001[b]
	Ot1:Positive (+): Sensorimotor	6.63	5.52	1.20	0.23
	Ot1:Negative (−):Sensorimotor	−4.04	5.52	−0.73	0.46
	Ot2:Positive (+):Sensorimotor	−16.55	5.90	−2.81	0.005[b]
	Ot2:Negative (−):Sensorimotor	−17.62	5.90	−2.99	0.003[b]
	Ot1:Cerebellar:Sensorimotor	4.69	5.61	0.83	0.40
	Ot2:Cerebellar:Sensorimotor	3.66	5.99	0.61	0.54
	Ot1:Cerebellar:Positive (+)	10.79	5.61	1.92	0.05
	Ot1:Cerebellar:Negative (−)	−0.74	5.61	−0.13	0.89
	Ot2:Cerebellar:Positive (+)	14.38	5.99	2.40	0.02[a]
	Ot2:Cerebellar:Negative (−)	14.39	5.99	2.40	0.02[a]
	Cerebellar:Positive (+):Sensorimotor	−1.53	0.85	−1.80	0.07
	Cerebellar:Negative (−):Sensorimotor	−0.20	0.85	−0,24	0.81
	Ot1:Cerebellar:Positive (+):Sensorimotor	−16.94	7.94	−2.13	0.03[a]
	Ot1:Cerebellar:Negative (−):Sensorimotor	10.62	7.94	1.33	0.18
	Ot2:Cerebellar:Positive (+):Sensorimotor	6.35	8.48	0.75	0.45
	Ot2: Cerebellar:Negative (−):Sensorimotor	11.87	8.48	1.40	0.16

[a] $P < 0.05$. [b] $P < 0.01$.

2018). Thanks to its cognitive contributions, feedforward models are used during task performance for learning. Thus, impaired inhibition in the cerebellar group may also contribute to this loop, selectively apparent during the negative tempi.

The results for tracking faster tempi were also inconsistent with our original hypothesis, which was based on a previous study suggesting that cerebellar patients experience difficulties in tracking fast tempi (Nozaradan et al. 2017). To elaborate, the authors compared neural encoding of the rhythm across cerebellar patients and HCs, based on the frequency-tagging approach, measuring the amplitude of the responses expected at frequencies corresponding to stimulation frequencies (Nozaradan 2014; Nozaradan et al. 2017). The study showed a reduced relative amplitude at beat frequency in the cerebellar patients especially at the fastest tempo (x4 of the original tempo)—which requires rapid and temporally precise event encoding. It is noteworthy that we cannot draw a direct comparison with our study, as they used a tempo with a factor of ×4 (Nozaradan et al. 2017), thus an extreme case, compared to our +10% of the original tempi of 100 beats per minute.

A dissociation was observed between the behavioral and neural responses. That is, while we observed a spared behavioral adaptation in cerebellar patients comparable to that of HCs, we found reduced neural tracking activity. Given that no group differences were observed in the tracking response of the finger-taps (i.e. behavioral ERFA) compared to that of the neural sensorimotor component ERFA, one may also argue that covert and overt processes may operate in parallel, utilizing different mechanisms to achieve alignment. This distinction could be explained by the task requiring two different intertwined temporal processing mechanisms based on event and continuous cyclic timing. The involvement of the cerebellum has been shown to be essential for event timing, where temporal information can be defined by isolated intervals (e.g. here, the perturbations) and is independent of whether the tasks are motoric or perceptual. In contrast, it has been shown that the cerebellum is not necessary when temporal information is defined by the dynamic, cyclic event (Ivry et al. 2002; Spencer et al. 2003; Teki et al. 2011; Breska and Ivry 2016). Moreover, the contribution of the motor system and higher-order top-down systems can also be weighed into temporal processing

(Rimmele et al. 2018) and temporal attention (Zalta et al. 2020). The motor system is critically implicated in timing and time perception (Coull et al. 2011; Teki et al. 2011; Kotz et al. 2016; Merchant and K. 2016) and periodic beat-based timing. Particularly, it is underpinned by striato-thalamo-cortical circuits. Studies have confirmed previous results showing that overt motor activity optimizes auditory periodic temporal attention (Morillon et al. 2014; Morillon and Baillet 2017). Furthermore, neural responses elicited in auditory cortical areas could be modulated by higher-level associative areas and/or motor areas (Patel and Iversen 2014; Large et al. 2015). For instance, temporally precise two-way communication between auditory and motor regions seemed to be occurring in the form of functional connections based on beat perception (Patel and Iversen 2014). Moving to another model, beat perception is proposed to be underpinned by neural entrainment at beat frequency emerging as the non-linear product of the coupling between the rhythmic auditory input and a network of neural non-linear oscillators within a network of sensory and motor areas (Large et al. 2015).

Overall, the evidence for preserved adaptation in cerebellar patients supports the idea that timing is mediated not by specific structures, but rather by functional neural networks including structures such as the cerebellum, basal ganglia, supplementary motor area and others (Coull et al. 2011; Mioni et al. 2020).

This finding is relevant, as rhythm-based interventions have been shown to improve movement coordination and timing accuracy, making them a promising tool for neurological rehabilitation (Rodriguez-Fornells et al. 2012; Schaefer 2014; Bella et al. 2017; Moumdjian et al. 2019; Hutchinson et al. 2020; Braun Janzen et al. 2021; Ruotsalainen et al. 2022). Therefore, the findings of our study suggest the potential to leverage rhythm-based interventions to enhance motor function in PwCI. We note, however, that our sample consisted of PwCI with mild impairment, so caution should be adopted to generalize these results to moderate or severe impairments.

Study limitations and future directions

A limitation of the present study is the significant age difference between the cerebellar and control groups. To account for this potential confound, we conducted additional analyses testing for age by group interaction effects on each ERFA measure (behavioral, perceptual, and sensorimotor), separately for positive and negative perturbation directions. As shown in Supplementary Table 1, none of the interactions reached statistical significance, indicating that the observed group differences in ERFA responses were not confounded by age. A limitation of ERFA lies in its applicability to different types of perturbations with different intrinsic characteristics. Specifically, ERFA is well-suited for perturbations that elicit sustained responses, such as period changes, as it effectively quantifies frequency adjustments over time, and thus conversely, it is less effective for transient responses.

ERFA, as an outcome to quantify behavioral and neural tracking of rhythmic stimuli, captured the adaptation processes taking place during the sensorimotor synchronization task. One may further expand these investigations to the underlying anticipation processes required during sensorimotor synchronization tasks. These can be computationally modeled to detail the predictive processes employed during the correcting of errors in response to the perturbations applied in this paradigm. One example of such a computational model is the Adaptation Anticipation model of sensorimotor synchronization (van der Steen and Keller 2013). The experimental paradigm can also be extended by including a perturbation paradigm within the listening task. While a paradigm as such holds methodological challenges, it may allow further refined comparisons between perceptual and sensorimotor components. Lastly, studies can investigate adaptation across groups according to task difficulty, such as by manipulating the magnitude of perturbations. This may provide additional fine-grained information regarding the role of the cerebellum in adaptation processes within sensorimotor synchronization tasks.

Conclusion

We observed spared mean behavioral tracking yet distinct neural tracking in PwCI, comparable to that of HCs when adapting to randomly occurring period perturbations in auditory metronomes. The neural sensorimotor component only significantly differentiated between groups, where patients showed worse tracking than HCs, especially for negative compared to positive directions. Given the spared mean behavioral adaptation abilities in the cerebellar patients, in contrast with the hindered neural dynamics, our results suggest the presence of parallel yet distinct mechanisms for processing of covert and overt responses underlying sensorimotor adaption.

Acknowledgments

We thank Ivan Schepers (IPEM, UGent) for his technical support in the development of the tapping pad equipment, Nele Vanbilsen's assistance and support with parts of data collection and all study participants for their voluntary participation in the study.

Author contribution

Eleonora Baliviera (Data curation, Formal analysis, Investigation, Methodology, Visualization, Writing—original draft, Writing—review & editing), Mattia Rosso (Conceptualization, Formal analysis, Methodology, Resources, Software, Validation, Visualization, Writing—review & editing), Bart Moens (Methodology, Resources, Software, Writing—review & editing), Marie Poncelet (Data curation, Investigation, Writing—review & editing), Mario Manto (Funding acquisition, Project administration, Resources, Supervision, Writing—review & editing), Pierre Cabaraux (Data curation, Project administration, Resources, Writing—review & editing), Bart Van Wijmeersch (Data curation, Funding acquisition, Resources, Writing—review & editing), Marc Leman (Conceptualization, Funding acquisition, Supervision, Writing—review & editing), Peter Feys (Conceptualization, Funding acquisition, Resources, Supervision, Validation, Writing—review & editing), and Lousin Moumdjian (Conceptualization, Data curation, Formal analysis, Funding acquisition, Investigation, Methodology, Project administration, Validation, Visualization, Writing—original draft, Writing—review & editing).

Supplementary material

Supplementary material is available at *Cerebral Cortex* online. Three supplementary materials are provided: (i) examples of the period perturbations in negative and positive directions, included as supplementary auditory files; (ii) Supplementary Fig. 1, illustrating the GED quality check; and (iii) Supplementary Table 1, reporting of summary statistics of age and group interaction on each ERFA outcome.

Funding

This work was supported by the Fonds Wetenschappelijk Onderzoek (FWO) (grant numbers 1295923N, G082021N) awarded to dr. Lousin Moumdjian, and Prof. Peter Feys, respectively.

Conflict of interest statement: Authors declare that they have no competing interests.

Data availability

The datasets used and/or analyzed during the current study are available from the corresponding author on reasonable request.

Ethics approval and consent to participate

This study was approved by the Medical Ethical Committee of Hasselt University and the local ethical committee of C.H.U. Charleroi and Erasme Hospital Brussels (B1152021000003), the National MS Center Melsbroek and the Rehabilitation and MS center Noorderhart (B1152020000011). All included participants provided their consent to participate by the means of written informed consent.

References

Band GP, van Boxtel GJ. 1999. Inhibitory motor control in stop paradigms: review and reinterpretation of neural mechanisms. *Acta Psychol*. 101:179–211. https://doi.org/10.1016/s0001-6918(99)00005-0.

Bares M et al. 2019. Consensus paper: decoding the contributions of the cerebellum as a time machine. From neurons to clinical applications. *Cerebellum*. 18:266–286. https://doi.org/10.1007/s12311-018-0979-5.

Bastian AJ. 2006. Learning to predict the future: the cerebellum adapts feedforward movement control. *Curr Opin Neurobiol*. 16:645–649. https://doi.org/10.1016/j.conb.2006.08.016.

Bella SD et al. 2017. Gait improvement via rhythmic stimulation in Parkinson's disease is linked to rhythmic skills. *Sci Rep*. 7:42005. https://doi.org/10.1038/srep42005.

Boashash B. 1992. Estimating and interpreting the instantaneous frequency of a signal. I. Fundamentals. *Proc IEEE*. 80:520–538. https://doi.org/10.1109/5.135376.

Braun Janzen T, Koshimori Y, Richard NM, Thaut MH. 2021. Rhythm and music-based interventions in motor rehabilitation: current evidence and future perspectives. *Front Hum Neurosci*. 15:789467. https://doi.org/10.3389/fnhum.2021.789467.

Breska A, Ivry RB. 2016. Taxonomies of timing: where does the cerebellum fit In? *Curr Opin Behav Sci*. 8:282–288. https://doi.org/10.1016/j.cobeha.2016.02.034.

Breska A, Ivry RB. 2018. Double dissociation of single-interval and rhythmic temporal prediction in cerebellar degeneration and Parkinson's disease. *Proc Natl Acad Sci USA*. 115:12283–12288. https://doi.org/10.1073/pnas.1810596115.

Cabaraux P et al. 2023. Consensus paper: ataxic gait. *Cerebellum*. 22:394–430. https://doi.org/10.1007/s12311-022-01373-9.

Cohen MX. 2014. Fluctuations in oscillation frequency control spike timing and coordinate neural networks. *J Neurosci*. 34:8988–8998. https://doi.org/10.1523/JNEUROSCI.0261-14.2014.

Cohen MX. 2022. A tutorial on generalized eigendecomposition for denoising, contrast enhancement, and dimension reduction in multichannel electrophysiology. *Neuroimage*. 247:118809. https://doi.org/10.1016/j.neuroimage.2021.118809.

Coull JT, Cheng RK, Meck WH. 2011. Neuroanatomical and neurochemical substrates of timing. *Neuropsychopharmacology*. 36:3–25. https://doi.org/10.1038/npp.2010.113.

Dhawale AK, Smith MA, Olveczky BP. 2017. The role of variability in motor learning. *Annu Rev Neurosci*. 40:479–498. https://doi.org/10.1146/annurev-neuro-072116-031548.

Gatti D, Rinaldi L, Ferreri L, Vecchi T. 2021. The human cerebellum as a hub of the predictive brain. *Brain Sci*. 11:1492. https://doi.org/10.3390/brainsci11111492.

Haegens S, Zion Golumbic E. 2018. Rhythmic facilitation of sensory processing: a critical review. *Neurosci Biobehav Rev*. 86:150–165. https://doi.org/10.1016/j.neubiorev.2017.12.002.

Hoche F, Guell X, Vangel MG, Sherman JC, Schmahmann JD. 2018. The cerebellar cognitive affective/Schmahmann syndrome scale. *Brain*. 141:248–270. https://doi.org/10.1093/brain/awx317.

Hutchinson K et al. 2020. A music-based digital therapeutic: proof-of-concept automation of a progressive and individualized rhythm-based walking training program after stroke. *Neurorehabil Neural Repair*. 34:986–996. https://doi.org/10.1177/1545968320961114.

Ivry RB, Spencer RM, Zelaznik HN, Diedrichsen J. 2002. The cerebellum and event timing. *Ann N Y Acad Sci*. 978:302–317. https://doi.org/10.1111/j.1749-6632.2002.tb07576.x.

Jantzen KJ, Ratcliff BR, Jantzen MG. 2018. Cortical networks for correcting errors in sensorimotor synchronization depend on the direction of asynchrony. *J Mot Behav*. 50:235–248. https://doi.org/10.1080/00222895.2017.1327414.

Kotz SA, Stockert A, Schwartze M. 2014. Cerebellum, temporal predictability and the updating of a mental model. *Philos Trans R Soc Lond Ser B Biol Sci*. 369:20130403. https://doi.org/10.1098/rstb.2013.0403.

Kotz SA, Brown RM, Schwartze M. 2016. Cortico-striatal circuits and the timing of action and perception. *Curr Opin Behav Sci*. 8:42–45. https://doi.org/10.1016/j.cobeha.2016.01.010.

Lakatos P, Gross J, Thut G. 2019. A new unifying account of the roles of neuronal entrainment. *Curr Biol*. 29:R890–R905. https://doi.org/10.1016/j.cub.2019.07.075.

Large EW, Snyder JS. 2009. Pulse and meter as neural resonance. *Ann N Y Acad Sci*. 1169:46–57. https://doi.org/10.1111/j.1749-6632.2009.04550.x.

Large EW, Herrera JA, Velasco MJ. 2015. Neural networks for beat perception in musical rhythm. *Front Syst Neurosci*. 9:159. https://doi.org/10.3389/fnsys.2015.00159.

Manto M. 2009. Mechanisms of human cerebellar dysmetria: experimental evidence and current conceptual bases. *J Neuroeng Rehabil*. 6:10. https://doi.org/10.1186/1743-0003-6-10.

Manto M et al. 2012. Consensus paper: roles of the cerebellum in motor control–the diversity of ideas on cerebellar involvement in movement. *Cerebellum*. 11:457–487. https://doi.org/10.1007/s12311-011-0331-9.

Marsden J, Harris C. 2011. Cerebellar ataxia: pathophysiology and rehabilitation. *Clin Rehabil*. 25:195–216. https://doi.org/10.1177/0269215510382495.

McLachlan NM, Wilson SJ. 2017. The contribution of brainstem and cerebellar pathways to auditory recognition. *Front Psychol*. 08:265. https://doi.org/10.3389/fpsyg.2017.00265.

Merchant HY, K. 2016. How the motor system both encodes and influences our sense of time. *Curr Opin Behav Sci*. 8:22–27. https://doi.org/10.1016/j.cobeha.2016.01.006.

Mioni G, Grondin S, Bardi L, Stablum F. 2020. Understanding time perception through non-invasive brain stimulation techniques:

a review of studies. *Behav Brain Res*. 377:112232. https://doi.org/10.1016/j.bbr.2019.112232.

Mirman D. 2017. *Growth curve analysis and visualization using R*. CRC Press, Boca Raton. 10.1201/9781315373218.

Mitoma H, Manto M, Hampe CS. 2018. Time is cerebellum. *Cerebellum*. 17:387–391. https://doi.org/10.1007/s12311-018-0925-6.

Molinari M, Leggio MG, Thaut MH. 2007. The cerebellum and neural networks for rhythmic sensorimotor synchronization in the human brain. *Cerebellum*. 6:18–23. https://doi.org/10.1080/14734220601142886.

Morillon B, Baillet S. 2017. Motor origin of temporal predictions in auditory attention. *Proc Natl Acad Sci USA*. 114:E8913–E8921. https://doi.org/10.1073/pnas.1705373114.

Morillon B, Schroeder CE, Wyart V. 2014. Motor contributions to the temporal precision of auditory attention. *Nat Commun*. 5:5255. https://doi.org/10.1038/ncomms6255.

Moumdjian L et al. 2019. Walking to music and metronome at various tempi in persons with multiple sclerosis: a basis for rehabilitation. *Neurorehabil Neural Repair*. 33:464–475. https://doi.org/10.1177/1545968319847962.

Nozaradan S. 2014. Exploring how musical rhythm entrains brain activity with electroencephalogram frequency-tagging. *Philos Trans R Soc Lond Ser B Biol Sci*. 369:20130393. https://doi.org/10.1098/rstb.2013.0393.

Nozaradan S, Peretz I, Missal M, Mouraux A. 2011. Tagging the neuronal entrainment to beat and meter. *J Neurosci*. 31:10234–10240. https://doi.org/10.1523/JNEUROSCI.0411-11.2011.

Nozaradan S, Peretz I, Mouraux A. 2012a. Selective neuronal entrainment to the beat and meter embedded in a musical rhythm. *J Neurosci*. 32:17572–17581. https://doi.org/10.1523/JNEUROSCI.3203-12.2012.

Nozaradan S, Peretz I, Mouraux A. 2012b. Steady-state evoked potentials as an index of multisensory temporal binding. *Neuroimage*. 60:21–28. https://doi.org/10.1016/j.neuroimage.2011.11.065.

Nozaradan S, Zerouali Y, Peretz I, Mouraux A. 2015. Capturing with EEG the neural entrainment and coupling underlying sensorimotor synchronization to the beat. *Cereb Cortex*. 25:736–747. https://doi.org/10.1093/cercor/bht261.

Nozaradan S, Schwartze M, Obermeier C, Kotz SA. 2017. Specific contributions of basal ganglia and cerebellum to the neural tracking of rhythm. *Cortex*. 95:156–168. https://doi.org/10.1016/j.cortex.2017.08.015.

Oostenveld R, Fries P, Maris E, Schoffelen JM. 2011. FieldTrip: open source software for advanced analysis of MEG, EEG, and invasive electrophysiological data. *Comput Intell Neurosci*. 2011:156869. https://doi.org/10.1155/2011/156869.

Oxford Grice K et al. 2003. Adult norms for a commercially available nine hole peg test for finger dexterity. *Am J Occup Ther*. 57:570–573. https://doi.org/10.5014/ajot.57.5.570.

Patel AD, Iversen JR. 2014. The evolutionary neuroscience of musical beat perception: the action simulation for auditory prediction (ASAP) hypothesis. *Front Syst Neurosci*. 8:57. https://doi.org/10.3389/fnsys.2014.00057.

Peretz I, Champod AS, Hyde K. 2003. Varieties of musical disorders. The Montreal battery of evaluation of Amusia. *Ann N Y Acad Sci*. 999:58–75. https://doi.org/10.1196/annals.1284.006.

Pollok B, Moll M, Schmitz F, Muller K, Schnitzler A. 2002. Rapid mapping of finger representations in human primary somatosensory cortex applying neuromagnetic steady-state responses. *Neuroreport*. 13:235–238. https://doi.org/10.1097/00001756-200202110-00012.

Popa LS, Ebner TJ. 2018. Cerebellum, predictions and errors. *Front Cell Neurosci*. 12:524. https://doi.org/10.3389/fncel.2018.00524.

Rajendran VG, Schnupp JWH. 2019. Frequency tagging cannot measure neural tracking of beat or meter. *Proc Natl Acad Sci USA*. 116:2779–2780. https://doi.org/10.1073/pnas.1820020116.

Repp BH. 2005. Sensorimotor synchronization: a review of the tapping literature. *Psychon Bull Rev*. 12:969–992. https://doi.org/10.3758/bf03206433.

Rimmele JM, Morillon B, Poeppel D, Arnal LH. 2018. Proactive sensing of periodic and aperiodic auditory patterns. *Trends Cogn Sci*. 22:870–882. https://doi.org/10.1016/j.tics.2018.08.003.

Rodriguez-Fornells A et al. 2012. The involvement of audio-motor coupling in the music-supported therapy applied to stroke patients. *Ann N Y Acad Sci*. 1252:282–293. https://doi.org/10.1111/j.1749-6632.2011.06425.x.

Rosso M, Leman M, Moumdjian L. 2021a. Neural entrainment meets behavior: the stability index as a neural outcome measure of auditory-motor coupling. *Front Hum Neurosci*. 15:668918. https://doi.org/10.3389/fnhum.2021.668918.

Rosso M, Maes PJ, Leman M. 2021b. Modality-specific attractor dynamics in dyadic entrainment. *Sci Rep*. 11:18355. https://doi.org/10.1038/s41598-021-96054-8.

Rosso M, Heggli OA, Maes PJ, Vuust P, Leman M. 2022. Mutual beta power modulation in dyadic entrainment. *Neuroimage*. 257:119326. https://doi.org/10.1016/j.neuroimage.2022.119326.

Rosso M, Moens B, Leman M, Moumdjian L. 2023a. Neural entrainment underpins sensorimotor synchronization to dynamic rhythmic stimuli. *Neuroimage*. 277:120226. https://doi.org/10.1016/j.neuroimage.2023.120226.

Rosso M, van Kerrebroeck B, Maes PJ, Leman M. 2023b. Embodied perspective-taking enhances interpersonal synchronization: a body-swap study. *iScience*. 26:108099. https://doi.org/10.1016/j.isci.2023.108099.

Ruotsalainen J, Carlson E, Erkkilä J. 2022. Rhythmic exercises as tools for rehabilitation following cerebellar stroke: a case study integrating music therapy and physiotherapy techniques. *Nord J Music Ther*. 31:431–453. https://doi.org/10.1080/08098131.2022.2026452.

Schaefer RS. 2014. Auditory rhythmic cueing in movement rehabilitation: findings and possible mechanisms. *Philos Trans R Soc Lond Ser B Biol Sci*. 369:20130402. https://doi.org/10.1098/rstb.2013.0402.

Schmahmann JD. 2019. The cerebellum and cognition. *Neurosci Lett*. 688:62–75. https://doi.org/10.1016/j.neulet.2018.07.005.

Schmitz-Hubsch T et al. 2006. Scale for the assessment and rating of ataxia: development of a new clinical scale. *Neurology*. 66:1717–1720. https://doi.org/10.1212/01.wnl.0000219042.60538.92.

Schwartze M, Keller PE, Kotz SA. 2016. Spontaneous, synchronized, and corrective timing behavior in cerebellar lesion patients. *Behav Brain Res*. 312:285–293. https://doi.org/10.1016/j.bbr.2016.06.040.

Spencer RM, Zelaznik HN, Diedrichsen J, Ivry RB. 2003. Disrupted timing of discontinuous but not continuous movements by cerebellar lesions. *Science*. 300:1437–1439. https://doi.org/10.1126/science.1083661.

Teki S, Grube M, Griffiths TD. 2011. A unified model of time perception accounts for duration-based and beat-based timing mechanisms. *Front Integr Neurosci*. 5:90. https://doi.org/10.3389/fnint.2011.00090.

van der Steen MC, Keller PE. 2013. The ADaptation and anticipation model (ADAM) of sensorimotor synchronization. *Front Hum Neurosci*. 7:253. https://doi.org/10.3389/fnhum.2013.00253.

van der Steen MC, Schwartze M, Kotz SA, Keller PE. 2015. Modeling effects of cerebellar and basal ganglia lesions on adaptation and anticipation during sensorimotor synchronization. *Ann N Y Acad Sci*. 1337:101–110. https://doi.org/10.1111/nyas.12628.

Vanbilsen N et al. 2023. Auditory attention measured by EEG in neurological populations: systematic review of literature and meta-analysis. *Sci Rep*. 13:21064. https://doi.org/10.1038/s41598-023-47597-5.

Voogd J. 2003. The human cerebellum. *J Chem Neuroanat*. 26:243–252. https://doi.org/10.1016/j.jchemneu.2003.07.005.

Zalta A, Petkoski S, Morillon B. 2020. Natural rhythms of periodic temporal attention. *Nat Commun*. 11:1051. https://doi.org/10.1038/s41467-020-14888-8.

Cerebral Cortex, 2025, **35**, bhaf164
https://doi.org/10.1093/cercor/bhaf164
Original Article